**communications** materials

**Article**

https://doi.org/10.1038/s43246-024-00549-6

# Optoelectronic properties of electron-acceptor molecules adsorbed on graphene/silicon carbide interfaces

**Masoud Mansouri[1] ✉, Cristina Díaz[2] & Fernando Martín[1,3]**

Silicon carbide has emerged as an optimal semiconducting support for graphene growth. In previous studies, the formation of an interfacial graphene-like buffer layer covalently bonded to silicon carbide has been observed, revealing electronic properties distinct from ideal graphene. Despite extensive experimental efforts dedicated to this interface, theoretical investigations have been confined to its ground state. Here, we use many-body perturbation theory to study the electronic and optical characteristics of this interface and demonstrate its potential for optoelectronics. By adsorbing graphene, we show that the quasiparticle band structure exhibits a reduced bandgap, associated with an optical onset in the visible energy window. Furthermore, we reveal that the absorption of two prototypical electron-accepting molecules on this substrate results in a significant renormalization of the adsorbate gap, giving rise to distinct low-lying optically excited states in the near-infrared region. These states are well-separated from the substrate's absorption bands, ensuring wavelength selectivity for molecular optoelectronic applications.

Silicon carbide (SiC) is an indirect semiconductor with partially ionic bonds that exhibits numerous polytypical forms, among them the hexagonal 4H and 6H ones[1–10]. The 4H and 6H polytypes are characterized by identical bilayers but possess distinct close-packed stacking sequences[3,10,11]. In addition to their relevance in electronics and industry[1–3,12], the high-temperature decomposition of 4H- and 6H-SiC provides a direct route to grow single or multi-layers of graphene (Gr)[13–19]. The resulting Gr adlayer on SiC holds significance in various fields, such as high-precision metrology, gas sensing, and high-frequency transistors[20–22], which explains the experimental efforts devoted to studying the growth of Gr on different polar faces of the SiC substrates[3,13,14,16,23]. This growth process initiates by forming a structurally graphene-like layer, commonly known as the interfacial buffer layer (BL), covalently bonded to the substrate. This BL exhibits electronic properties remarkably different from those of ideal Gr, including the existence of a sizeable bandgap at the Dirac points and the absence of the characteristic $\pi$-band[3,22].

The formation of the BL on the Si-terminated (0001) or C-terminated $(000\bar{1})$ faces is associated with qualitatively different electronic structures: while previous studies[24,25] have shown that the former features a metallic characteristic of the interface by crossing the Fermi level, the latter retains the semiconducting nature of the substrate, which is of particular interest to produce viable semiconducting graphene[16]. Concerning the geometric structure of the interface, it has been concluded that graphitization on SiC (0001) occurs with a complex $(6\sqrt{3}\times6\sqrt{3})$R30 periodicity[20,24], whereas high-quality Gr islands with larger domain sizes and significantly improved electron mobilities[26] form on the C-terminated SiC$(000\bar{1})$ with a reconstruction of $(\sqrt{3}\times\sqrt{3})$R30[13,15,17,23,25]–shortly $\sqrt{3}$R. Given the advantageous unit-cell size and superior electron mobility of the latter[13,25], our study delves into the electronic structure and optical properties of the Gr/SiC$(000\bar{1})$ system.

Previous experiments have established that BL/SiC serves as an ideal substrate for the epitaxial growth of ensuing Gr layers with uniform thickness[13,15,20]. These overlying layers acquire the characteristic electronic structure associated with pristine Gr, indicative of weak interaction with the BL/SiC substrate[13,20,24–26]. Furthermore, the BL/SiC substrate holds the potential for serving as a support for adsorbing molecules, thereby opening avenues for novel applications in quantum information technology[27] and biosensors[28]. Generally, the injection of holes by adsorbing molecular acceptors has been identified as a simple and reliable technique for controlling the concentration of charge carriers at different interfaces[29–32]. In this work, we explore the adsorption of the molecular acceptors tetracyanoquinodimethane (TCNQ) and 2,3,5,6-tetrafluoro-tetracyanoquinodimethane (F4TCNQ) onto the semiconducting BL/SiC$(000\bar{1})$ substrate. Charge-transfer driven by these adsorbates, known for their strong electron-

---

[1] Departamento de Química, Módulo 13, Universidad Autónoma de Madrid, Madrid 28049, Spain. [2] Departamento de Química Física, Facultad de CC. Químicas, Universidad Complutense de Madrid, Madrid 28040, Spain. [3] Instituto Madrileño de Estudios Avanzados en Nanociencia (IMDEA Nano), Campus de Cantoblanco, Madrid 28049, Spain. ✉e-mail: masoud.mansouri@uam.es

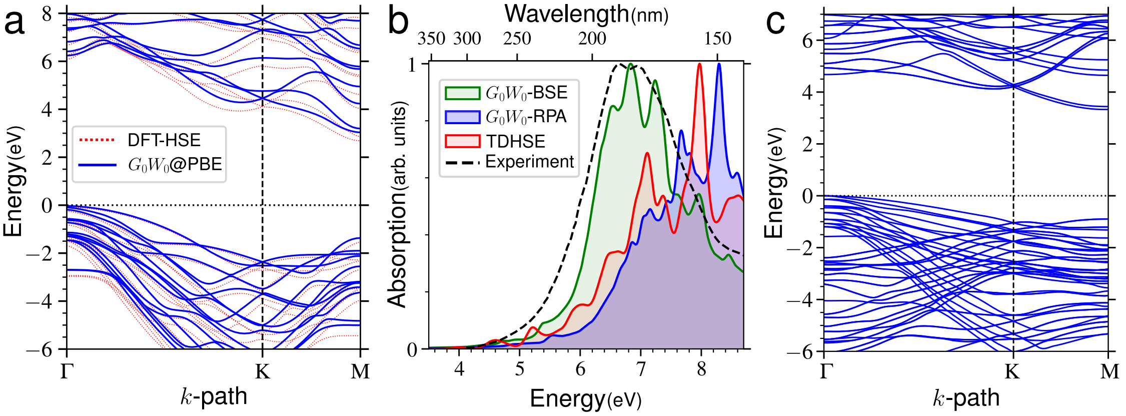

**Fig. 1 | Electronic structure and optical properties of 6H-SiC. a** The band structure and **b** the optical absorption spectra of the bulk. The experimental absorption spectrum was adapted from ref. 5 and shown by the black dashed line. To mimic the experimental resolution, theoretical spectra are broadened with a Lorentzian factor of 0.08 eV. **c** The quasiparticle band structure of the corresponding H-saturated surface. The valence band maximum is set to zero energy in the band structures.

accepting behavior and high electron affinities, is commonly utilized in Gr[29–34]. Particularly, the p-type doping of Gr with F4TCNQ, due to its enhanced interaction with surfaces attributed to the fluorinated structure and anchored nitrogen atoms, has been widely regarded as a promising method for compensating excess negative charge in epitaxial monolayer Gr[29,32–34]. Modification of the optoelectronic properties of Gr/SiC interfaces upon the adsorption of these acceptor molecules offers valuable insights into interface engineering, paving the way for the advancement of novel electronic and optoelectronic devices. When a molecule interacts with a surface, the self-consistent interaction induces a rearrangement of electron density, altering the alignment of frontier orbital energies and leading to a substantial reduction in the adsorbate gap compared to that of the gas phase[35]. For the two studied electron-accepting molecules, we demonstrate that this renormalization of the adsorbate gap on the substrate leads to the emergence of molecular states within the substrate gap. These states may act as trap levels for charge carriers, introducing new optically excited states and thereby enhancing the versatility of the substrate in optoelectronics.

Despite the above-mentioned experimental efforts devoted to exploiting the unique features of Gr/SiC and their relation with the polytypic character[22], current computational studies of the electronic structure of this system primarily rely on standard density functional theory (DFT)[23–25]. To achieve a more quantitative understanding of the intricate electronic interactions and excitations within this system, higher-level calculations based on many-body perturbation theory (MBPT) become crucial. In this work, we have used Green's function-based *GW* approach[36] in combination with a solution of the Bethe–Salpeter equation (BSE)[37]. These MBPT approaches are known for their accuracy in providing excitation energies, often aligning well with experimental photoemission and optical absorption spectra in both isolated and extended phases[37]. It is worth noting that the MBPT technique has already been applied in investigating the optoelectronic properties of pristine SiC bulks[4,7,8], nanoribbons[38,39], and defected SiC polytypes in bulk[12] and monolayers[40].

The paper is organized as follows. First, we validate our approach by comparing the calculated quasiparticle energies and optical absorption spectra for both 4H- and 6H-SiC in bulk and surface configurations with existing theoretical and experimental data. Then, we delve into the spin-polarized electronic structure of Gr adsorbed on both SiC (000$\bar{1}$) polytypes, revealing the presence of a singly occupied band within the intrinsic gap of the SiC substrate, accompanied by optically excited states within the visible energy window. Finally, we present our results for the adsorption of the two strong electron-accepting molecules TCNQ and F4TCNQ. Through a comparative analysis with the energy levels of isolated molecules, we demonstrate a notable renormalization of the adsorbate gap, leading to the emergence of a set of low-lying excited states in the near-infrared (NIR) region. These optically excited states, distinct from the absorption spectra bands of the substrate, provide the desired wavelength selectivity essential for potential applications in molecular optoelectronics.

## Results and discussion

### SiC bulk and surface

The geometry of bulk 4H-SiC and 6H-SiC was adopted from experimental data[1,41], as detailed in Supplementary Note 2. Employing the relaxed geometry obtained from DFT using the Heyd–Scuseria–Ernzerhof (HSE) hybrid functional, we initially explored the electronic structure and optical properties of both polytypes through the DFT-HSE (and its time-dependent extension, i.e., TDHSE) and *GW*-BSE approaches, assessing the accuracy of these theoretical methods in comparison to available experimental data. We should note that *GW* calculations in this study are performed using the perturbative one-shot ($G_0W_0$) scheme[37], utilizing the Perdew-Burke-Ernzerhof (PBE) orbitals and eigenvalues to construct non-interacting Green's functions $G_0$, with a screened interaction $W_0$ approximated at the random phase approximation (RPA) level[37].

The quasiparticle band structure of bulk 6H-SiC, shown in Fig. 1a, exhibits p-state characteristics of dispersive bands at edges. The $G_0W_0$@PBE calculations predict a band gap of 3.11 eV, which agrees well with the experimental value 3–3.05 eV[1,6–10]. The DFT-HSE estimates a smaller bandgap of 2.75 eV (see details in Supplementary Table 1). The same pattern can be seen in the corresponding optical absorption spectra depicted in Fig. 1b. The $G_0W_0$-BSE results (green-shaded) are in excellent agreement with the experiment[5], in contrast with those from $G_0W_0$-RPA (non-interacting, blue shaded area) and TDHSE (shaded-red). The latter two are qualitatively similar: they predict a maximum absorption at higher energies than the experiment, with TDHSE peaks consistently redshifting with respect to $G_0W_0$-RPA ones, mainly due to differences in direct gap energies. The introduction of excitonic effects through $G_0W_0$-BSE (green-shaded) results in a broader and more redshifted spectrum. The most important excitonic contribution appears in the 6–7.5 eV range. This is accompanied by a relatively weaker red shift in the near ultraviolet (UV) region with an onset of 4.23 eV that implies a small exciton binding energy ($\varepsilon_b$) of 230 meV. Inspecting the exciton wave function for the lowest bright transition reveals Mott–Wigner-like characteristics[37], delocalized across the unit cell.

For the H-saturated surface of $\sqrt{3}$R 6H-SiC, as illustrated in Supplementary Fig. 4, the quasiparticle band structure obtained at the $G_0W_0$@PBE level is shown in Fig. 1c. As can be seen, it exhibits a comparable $\Gamma \rightarrow M$ indirect bandgap, prominently featuring contributions from $C_p$ states in the valence manifold and a mixture of $Si_p$ and $C_s$ states at the conducting band-edge. Notably, the indirect gap is slightly widened with a value of 3.3 eV, whereas the direct gaps, particularly at the Γ-point, are narrowed compared to the corresponding bulk values (see Supplementary Table 1 for direct gaps). These changes are attributed to alterations in dielectric screening and broken symmetry resulting from surface reconstruction. Considering the reduction in the direct gaps, the optical absorption shown in Supplementary Fig. 9 indicates an energy onset of 3.6 eV, still within the UV region, with a more robust $\varepsilon_b$ of 0.5 eV. Previous experimental measurements at room temperature suggest an optical-bandgap energy for the slab of 6H-SiC in the range of 3–3.2 eV[6,42]. Recent studies have also demonstrated the temperature-dependent renormalization effects on the electronic structure[10] and optical properties[7] of both 6H- and 4H-SiC crystals.

Quasiparticle and optical spectra for 4H-SiC, both in bulk and surface phases, elaborated in Supplementary Note 3. As for the bulk, $G_0W_0$@PBE estimates an indirect quasiparticle gap of 3.29 eV with a BSE-onset of approximately 4.3 eV, corresponding to the direct gap of 4.56 eV at the M-point. These values are slightly larger than those of the 6H-SiC counterpart, in agreement with previous measurements[1,6,10]. The optical absorption of the $\sqrt{3}$R 4H-SiC surface in Supplementary Fig. 9 also reveals a notable resemblance to the 6H-SiC surface with a marginal redshift of 0.2 eV, mostly attributed to differences in direct gap energies.

## Graphene Adlayer on SiC (000$\bar{1}$)

Through high-resolution transmission electron microscopy, the 6H-SiC configuration has been identified as the preferred stacking for Gr growth[43]. Here, we investigate the electronic structure of a single Gr adlayer (or BL) on the 6H-SiC (000$\bar{1}$) surface—a parallel discussion for 4H-SiC is available in Supplementary Note 4.

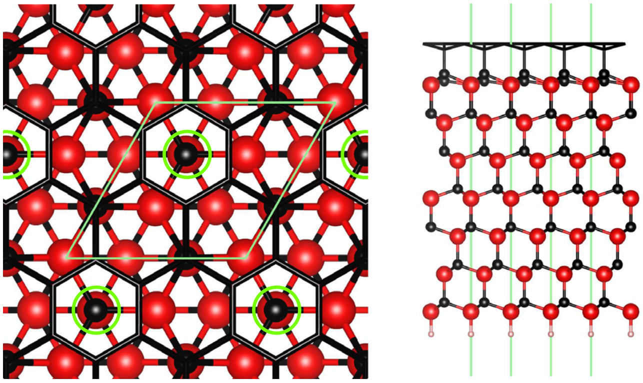

**Fig. 2 | Top and side views of the Gr adlayer on SiC (000$\bar{1}$).** Green circles highlight the $C_D$ atoms at the interface, and the green hexagon reveals the $\sqrt{3}$R reconstruction of the interface. Si, C, and H atoms are represented by red, black, and pink circles, respectively, with the Gr structure illustrated in a black-stick model.

A 2 × 2 reconstruction of multilayer Gr on the $\sqrt{3}$R 6H-SiC (000$\bar{1}$) surface has been previously observed through LEED[15] and X-ray[13] experiments. Consistent with these observations and previous theoretical studies[13,15,17,23,25], our Gr/SiC model used in this study comprises four Gr unit cells interfaced with three carbon atoms from the $\sqrt{3}$R 6H-SiC (000$\bar{1}$). Since the interaction among interface-derived states can vary concerning the stacking order and interface geometry, we have investigated multiple stacking configurations, illustrated in Supplementary Figs. 10 and 11. For the most energetically stable stacking, shown in Fig. 2, two carbon atoms of SiC (000$\bar{1}$) at the interface form direct bonds with Gr atoms while the third atom remains unbound and is positioned at the hollow site of Gr, referred to as the C-deficient atom ($C_D$). Consequently, the $C_D$ atom introduces a dangling bond with an unpaired electron that extends toward Gr. Given this, the DFT-HSE optimized geometry indicates that the substrate C-bonded atoms relax towards Gr with a bond length of 1.62 Å, in perfect agreement with experimental observations[13]. Such a bond length, which is slightly larger than that of a diamond, implies a strong interaction between Gr and the substrate[13]. In contrast, unbounded C atoms at the interface relax outward, giving rise to an average separation of 2.45 Å between Gr and the substrate. As a result, the interface displays a nonplanarity with a slight disorder of ~0.4 Å on either side.

The spin-polarized band structures depicted in Fig. 3a, calculated using DFT-HSE and $G_0W_0$@PBE methods, exhibit qualitatively similar characteristics, with an electronic band gap of approximately 2.4 and 2.8 eV for the minority and majority spin channels, respectively (see direct gaps in Supplementary Table 2). When compared to the band structure of bulk and pristine surface phases in Fig. 1, it is evident that, although the insulating character of the SiC substrate is retained, the direct gaps are significantly reduced. The main reason for this reduction is the emergence of a singly occupied state, primarily originating from the $C_D$ dangling bond within the interface. Considering the strongly localized character of this state, associated with a magnetic momentum of 1 $\mu_B$, the localization favors the spin polarization and gives rise to the splitting of this in-gap state[25]. This splitting is practically the same for DFT-HSE and $G_0W_0$@PBE calculations, although the two calculations differ by about 0.4 eV for the lower valence (higher conduction) bands, mainly influenced by the p-states of the SiC surface (Gr layer).

Figure 3b presents the optical absorption spectra of Gr/6H-SiC (000$\bar{1}$). Notably, the optical structures at the TDHSE and $G_0W_0$-BSE levels are qualitatively similar, in particular for the series of excitations across the visible energy window and the appearance of a dominant peak in the UV region. Over the visible energy range, TDHSE estimates an optical gap of 2.38 eV, arising from spin-down transitions between the SiC valence states and the in-gap $C_D$-induced state. This is followed by a relatively robust

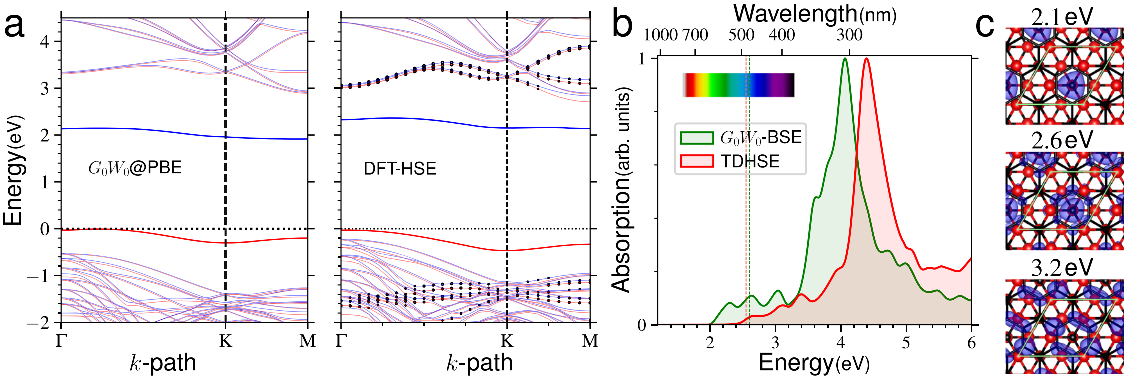

**Fig. 3 | Electronic and optical properties of Gr on 6H-SiC (000$\bar{1}$).** **a** Spin-polarized band structures obtained via two theoretical approaches. Spin majority and minority are represented in red and blue, respectively, with the valence band maximum set to zero energy. The contribution of the Gr adlayer within the DFT-HSE band structure is marked by black circles, magnified by a factor of 10 for clarity. **b** The corresponding optical absorption spectra are normalized and broadened with a Gaussian factor of 0.08 eV. The vertical green and red dashed lines indicate the direct gap estimated by $G_0W_0$@PBE and DFT-HSE calculations. **c** The isosurface of the exciton wave function for the three states discussed in the text.

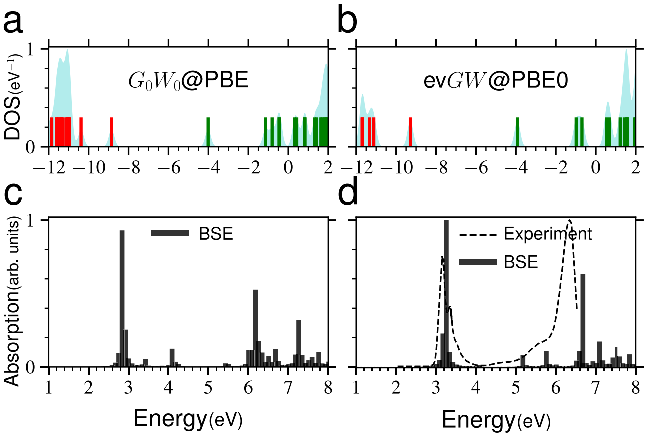

**Fig. 4 | Quasiparticle spectra and absorption lines for the isolated TCNQ molecule.** Panels **a** and **b** exhibit the quasiparticle energies (occupied: red bars, unoccupied: green bars) computed using the $G_0W_0$@PBE and ev$GW$@PBE0 approaches, respectively. **c** and **d** show the corresponding BSE solutions. The experimental UV–visible absorption spectrum in **d**, indicated by the black dashed line, is adapted from ref. 48.

transition at 2.73 eV, originating from the $C_D$-induced occupied state to the conducting manifold (see the coupling coefficients of electron–hole pairs associated with these two prominent bright states in Supplementary Fig. 13). On the other hand, the $G_0W_0$-BSE spectrum displays a significant redshift across the visible energy window with an optical gap of 2.06 eV, suggesting a stronger $\varepsilon_b$ of 550 meV. The most important transitions predicted by $G_0W_0$-BSE in this energy region appear at 2.1, 2.6, and 3.2 eV. Analyzing the corresponding exciton wave functions, depicted in Fig. 3c, reveals that the excitation at 2.1 eV is predominantly localized around the $C_D$ atom, while that at 2.6 eV additionally involves the contribution of the Gr layer, pointing out transitions between the singly occupied band and the hybridized conducting edge. As for the 3.2-eV excitation, the contribution of the Gr layer is even more evident; it originates from transitions between the spin-down valence edge and the hybridized Gr/SiC conduction edge.

## Adsorption of electron acceptor molecules

Considering the need for a relatively large supercell to investigate the adsorption of the TCNQ and F4TCNQ molecules, we have initially conducted an electronic structure benchmark for the reconstructed $\sqrt{3}$R Gr/6H-SiC (000$\bar{1}$) models consisting of three to seven SiC bilayers. Our detailed analysis, outlined in Supplementary Note 5, demonstrates minimal variations in the DFT-PBE bandgap (of the order of a few hundredths of an eV) and band-edge shape across models with different SiC bilayer numbers. This suggests a reasonably consistent electronic structure near band edges among models with different SiC bilayers. For subsequent MBPT calculations, we therefore opted for a three-SiC-bilayer supercell model as a sensible approximation to the actual system. Given the structural similarity between the 4H-SiC and 6H-SiC polytypes within the geometry of the first three SiC bilayers (see Supplementary Fig. 4), we can also extend our conclusions to the case of Gr/4H-SiC (000$\bar{1}$). Consequently, we omit polytype indications (4H and 6H) from the SiC designation in subsequent discussions. Further investigations into the adsorption energy and molecular geometry concerning supercell size, moreover, indicated that a 3 × 2 supercell of the $\sqrt{3}$R reconstruction is sufficient to minimize interactions among periodic images of adsorbates, thus providing a good balance between precision and computational cost. By using such a supercell, the minimum separation among periodic images of the adsorbates is ≈5.3 Å.

Exploring various adsorption sites on Gr/SiC(000$\bar{1}$), the most energetically favorable configuration for the two studied electron acceptors is illustarted in Supplementary Figs. 5 and 6. Upon full geometry optimization, both studied adsorbates adopt an almost planar structure, with a slight bending of N atoms toward the substrate, maintaining an average separation of 3.4 Å from the Gr layer. These structural characteristics are consistent with previous studies on the adsorption of these two molecules onto the ideal Gr layer[32,34]. The calculated adsorption energies[44] for TCNQ and F4TCNQ are −0.52 and −0.78 eV, respectively, which are not significantly different from those reported for other Gr substrates[33,34]. Furthermore, the negative values indicate the thermodynamic stability of the adsorption configuration. A Bader charge population analysis estimates a donation of 0.18 and 0.23 electrons from the substrate to the TCNQ and F4TCNQ molecules, respectively, confirming their electron-accepting characteristic at the interface.

The electronic structure and optical properties of TCNQ in the gas phase (i.e., a single free-standing molecule) are shown in Fig. 4. In the quasiparticle spectra of an isolated molecule, the negative energies of the highest occupied molecular orbital (HOMO) and lowest unoccupied molecular orbital (LUMO) could be interpreted as the ionization energy (IE) and electron affinity (EA), respectively[37,45]. At the $G_0W_0$@PBE level, the quasiparticle DOS indicates a HOMO–LUMO gap of 4.84 eV, with IE and EA of 8.85 and 4.01 eV, respectively. A comparison of these $G_0W_0$@PBE results with those obtained from the eigenvalue-only self-consistent $GW$ (ev$GW$) scheme, widely recognized for its reliability in dealing with organic molecules[37,46,47], reveals a minor difference in the LUMO energy, which is crucial for potential p-type coupling with surface states. In terms of the IE, however, the estimation of the ev$GW$ is 9.29 eV, showing a larger discrepancy of 0.44 eV concerning the $G_0W_0$@PBE-IE. Using the $G_0W_0$@PBE and ev$GW$@PBE0 quasiparticle energies, the corresponding BSE adsorption lines exhibit optical gaps of 2.86 and 3.23 eV, respectively. The latter agrees well with the gap observed in the UV–visible absorption spectrum (shown by the black dashed line in Fig. 4d), which is 3.17 eV[48]. Given this benchmark, therefore, one can anticipate an underestimation of ≈0.5 eV in the transport and optical gaps within the $G_0W_0$@PBE results due to the lack of self-consistency and the consequent starting-point dependence[37,45,46].

In the case of TCNQ/Gr/SiC(000$\bar{1}$), the DFT-PBE orbitals shown in Fig. 5a confirm that the LUMO of the adsorbate remains pure and localized on the molecule. This indeed aligns with the quasiparticle band structure in panel b, where the LUMO of the molecule, located at 1.8 eV, remains unoccupied with no dispersion. On the other hand, the HOMO of the adsorbate appears in the valence manifold at around −1.2 eV, hybridized with a few substrate states. Consequently, the adsorbate gap is determined to be 3 eV, reduced by about 1.84 eV compared to the gas-phase gap at the same level of theory. It is important to note that the quality of the discussed PBE orbitals, particularly those with adsorbate characteristics, is comparable to that of the DFT-HSE calculations.

The renormalization of the adsorbate gap, associated with the emergence of the adsorbate LUMO in the surface transport gap acting as a localized trap center, introduces a notable new feature in the optical structure of TCNQ/Gr/SiC compared to that of pristine Gr/SiC: the appearance of a set of low-lying-energy excitations within the NIR region (see panel c in Fig. 5). Analyzing the exciton wave functions over this region, particularly for the onset occurring at 0.92 eV, reveals a highly localized Frenkel-like characteristic around the adsorbate. This suggests that these excited states originate from transitions between the adsorbate HOMO, which is hybridized with multiple states of the substrate, and the LUMO. Compared to the gas-phase optical gap of 2.86 eV with an $\varepsilon_b$ of ~2 eV (obtained at the same level of theory, BSE using $G_0W_0$@PBE energies, see Fig. 4c), the adsorbate maintains its optical properties, with a similarly strong $\varepsilon_b$ that reduces the adsorbate gap of 3 eV to the optical onset at 0.92 eV. Within the visible energy window, the optical structure of TCNQ/Gr/SiC is qualitatively similar to that of the pristine substrate with an intensity enhancement, particularly between 2.5 and 2.8 eV. For the pristine substrate, the exciton wavefunction at 2.5 eV (shown in Fig. 5d with orange isosurface) involves transitions to the $C_D$ states and the conduction band-edge with Gr characteristics, which is consistent with results revealed in Fig. 3c. For the substrate involving the adsorbate, although the same excitation with only $C_D$ characteristics is found for the transition at 2 eV, the excitation at higher energies additionally involves a partial contribution of the adsorbate LUMO

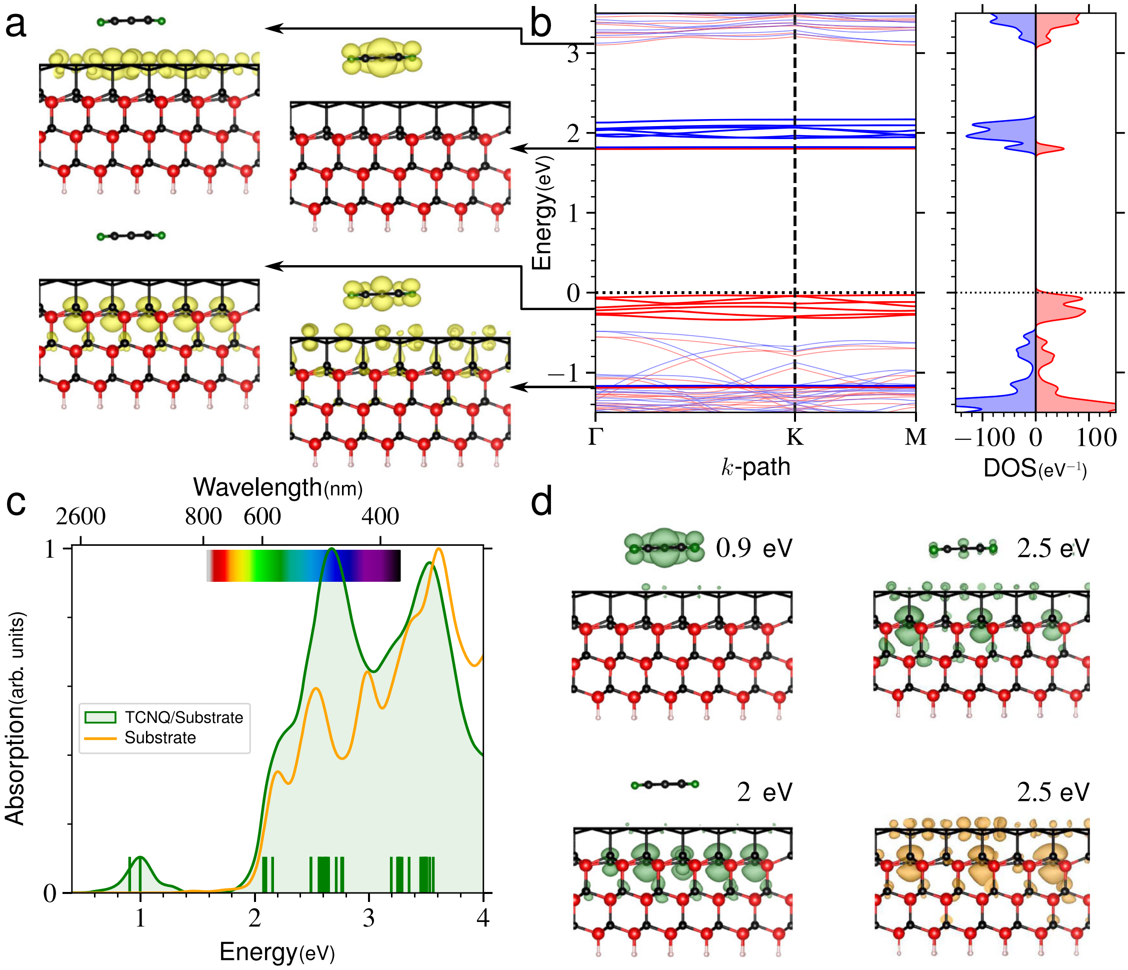

**Fig. 5 | Electronic structure and optical properties of TCNQ adsorbed on Gr/SiC (000$\bar{1}$) substrate. a** Spatial distribution of Kohn–Sham orbitals, including bands hybridized with the HOMO of TCNQ, the $C_D$ states at the valence edge, the LUMO of the molecule, and the lowest conduction bands. **b** Spin-polarized quasiparticle band structure and DOS, with spin majority and minority represented in red and blue. In addition to the six bands induced by the $C_D$ atoms at the interface, the frontier orbitals of TCNQ are illustrated in bold. **c** Absorption spectra for the substrate with and without the TCNQ adsorbate. Vertical green bars represent transitions with oscillator strength >0.1 of the strongest. **d** Isosurface of a few exciton states for the substrate with (green) and without (orange) the TCNQ adsorbate.

(e.g., see exciton at 2.5 eV with green isosurface). This implies that the enhancement is caused by partially allowed transitions from a few substrate states hybridized with the adsorbate HOMO to the LUMO.

For the adsorption of the F4TCNQ molecule on the Gr/SiC (000$\bar{1}$) surface, the electronic structure and optical properties are depicted in Fig. 6. Comparing it to the TCNQ case, the spatial distribution of the DFT-PBE orbitals suggests that the adsorbate HOMO is more significantly hybridized with substrate states, while its LUMO remains predominantly pure. Within the quasiparticle band structure, the LUMO and HOMO of the adsorbed F4TCNQ molecule are found at 1.55 and $\approx -1.3$ eV, respectively. As a result, the adsorbate gap is determined to be 2.85 eV, reduced by 1.82 eV compared to the isolated free-standing molecule, shown in Supplementary Fig. 15. Consequently, the corresponding absorption spectrum reveals a set of optically excited states within the NIR region. Specifically, strong transitions at about 0.8 eV, shown in Fig. 6d, feature the characteristics of the adsorbate LUMO, whereas the corresponding excitation for the isolated molecule occurs at 2.74 eV (see Supplementary Fig. 15). Upon adsorption, therefore, a similar renormalization of both the transport and optical gaps of the adsorbate is evident due to surface screening. Over the visible energy range, absorption spectra exhibit a significant increase between 2.5 and 3 eV upon the adsorption of the F4TCNQ molecule, accompanied by a slight redshift attributed to subtle modifications in the surface states. The analysis of the exciton wave functions in this region reveals robust transitions at 2.6 and 2.9 eV with notable contributions from the substrate, Gr and $C_D$ states in particular, associated with the adsorbate LUMO. Given the hybridization of multiple Gr/SiC states with the adsorbate's HOMO, the enhancement of the absorption intensity over the visible window can be attributed to the secondary allowed transitions to the adsorbate LUMO. Additionally, the deeper HOMO of F4TCNQ introduces a blueshift in the spectral peak at 2.9 eV compared to the TCNQ counterpart.

## Conclusion

Using the *GW* approach in the framework of MBPT, we have performed a detailed investigation of the spin-polarized electronic structure of graphene (Gr) adsorbed on both 4H- and 6H-SiC (000$\bar{1}$) surfaces. Our results reveal that the adsorption of Gr preserves the semiconducting characteristics of the SiC (000$\bar{1}$) surface, maintaining an appreciable band gap of 2.4 eV. Notably, a singly occupied band emerges within the intrinsic gap of the SiC substrate, significantly decreasing the direct gaps. The corresponding adsorption spectra show that the lowest optically excited state in both polytypes involves this in-gap state, leading to a clear trace in the visible energy window at about 2–3 eV.

We have also investigated the adsorption of TCNQ and F4TCNQ electron acceptors on the Gr/SiC (000$\bar{1}$) surface. Our results for both molecules demonstrate that although the adsorbate LUMO remains primarily localized on the molecule, its HOMO overlaps with multiple surface states, resulting in charge transfer from the substrate to the adsorbate. Compared to the quasiparticle spectra of the isolated molecules, we have

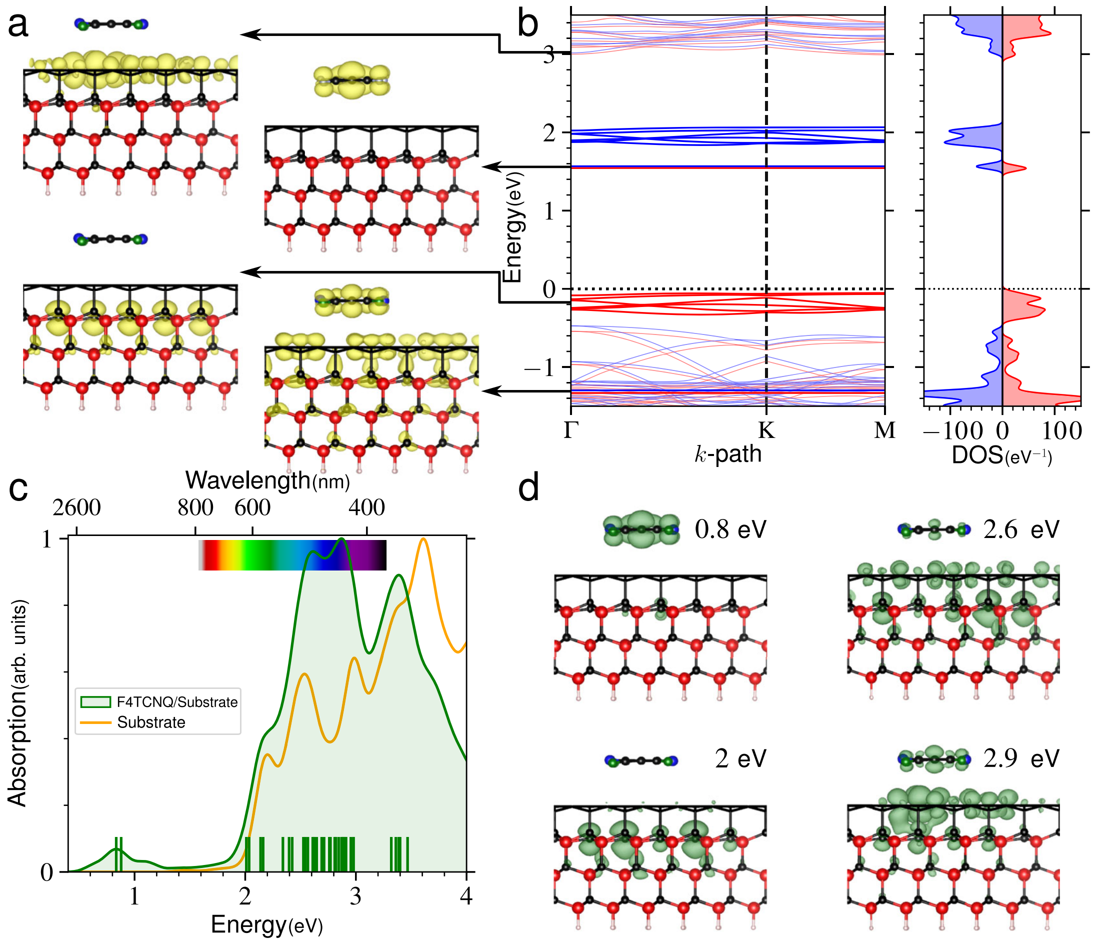

**Fig. 6 | Electronic structure and optical properties of the F4TCNQ/Gr/SiC(000$\bar{1}$).** **a** Spatial distribution of orbitals hybridized with the HOMO of the adsorbate, the $C_D$ states at the valence edge, the LUMO of the molecule, and the lowest conduction bands. **b** Quasiparticle band structures and **c** the corresponding BSE absorption spectra. **d** Exciton wavefunction for four discussed transitions in the text.

found a significant reduction of the adsorbate gaps (by ≈1.8 eV) due to surface screening. This renormalization of the adsorbate gap leads to the emergence of a set of optically excited states in the NIR region of the corresponding adsorption spectra, with a dominant contribution of the adsorbate LUMO. The appearance of distinct absorption bands in the NIR region upon adsorption of electron-accepting molecules is a very appealing feature for potential applications of Gr/SiC interfaces in molecular optoelectronics, offering new alternatives for future advancements in this field.

## Methods

Collinear spin-polarized DFT and time-dependent calculations were performed using VASP package[49]. In modeling the exchange-correlation potential, the hybrid HSE functional[50] with a 25% inclusion of exact exchange and a range separation parameter of 0.2 $Å^{-1}$ was used. We employed projector augmented wave potentials[51] to describe the core electrons, and the Grimme-D3 scheme[52] to account for van der Waals interactions. For surface (bulk) systems, we applied a plane-wave cutoff of 400 eV and a Γ-centered $6 \times 6 \times 1$ ($9 \times 9 \times 9$) sampling of the Brillouin zone, achieving convergence of the total energy to better than 0.05 meV. Geometry optimizations followed the same parameters, converging total energy and inter-atomic forces to less than $10^{-4}$ and 0.01 eV $Å^{-1}$, respectively. TDHSE spectra were computed using 12 occupied and 10 virtual bands, providing a sufficiently large energy window. For charge population analyses, we employed the Bader approach as implemented in ref. 53, accounting for both core and valence electron densities.

For MBPT calculations, the required DFT solutions were obtained using the QUANTUM ESPRESSO package[54], employing the PBE functional and norm-conserving pseudopotentials with scalar relativistic and core corrections[55]. The convergence of the ground-state total energy was thoroughly examined (see Supplementary Note 1). The $G_0W_0$ quasiparticle and optical absorption spectra were computed using the BERKELEYGW suite[56], with the frequency dependence of the dielectric function treated within the plasmon-pole model[37]. For bulks and surfaces, the dielectric matrix and self-energy were calculated using Brillouin-zone sampling grids of $6 \times 6 \times 3$ and $6 \times 6 \times 1$, respectively. Convergence tests in Supplementary Fig. 2, indicate that an energy cutoff of 18 (24) Ry for the dielectric, along with about 2350 (2700) empty bands, converges the transport gap within 0.01 eV for the studied surface (bulk) system. For molecular adsorption on the Gr/SiC supercell, the dielectric matrix was computed using a $2 \times 2 \times 1$ sampling and a cutoff of 14 Ry with at least 2500 bands, covering ≈35 eV above the Fermi energy. Optical absorption and excitonic properties were obtained by solving the BSE within the Tamm–Dancoff approximation[37,57]. The BSE kernel was interpolated to a finer Brillouin zone sampling: $9 \times 9 \times 6$ for SiC bulks, $10 \times 10 \times 1$ for Gr/SiC surfaces, and $8 \times 8 \times 1$ for surfaces with an adsorbate. The convergence of the absorption spectra concerning the number of valence and conduction bands in the expansion of the BSE kernel is provided in Supplementary Fig. 3.

Gas-phase calculations were conducted using the all-electron MOLGW code[58] and a cc-pVQζ basis set. In addition to the perturbative $G_0W_0$ scheme, we utilized the ev*GW* scheme, where the self-energy was initially constructed based on the hybrid PBE0 solutions. Subsequently, the *GW* correction was iteratively applied until the gap converged with an accuracy better than 0.01 eV.

## Data availability

Derived data supporting the findings of this study are available from the corresponding author upon reasonable request.

Received: 6 March 2024; Accepted: 20 June 2024;

## References

1. Levinshtein, M. E., Rumyantsev, S. L. & Shur, M. S. *Properties of Advanced Semiconductor Materials: GaN, AIN, InN, BN, SiC, SiGe* (John Wiley & Sons, 2001).
2. Zangooie, S. & Arwin, H. Surface, pore morphology, and optical properties of porous 4H-SiC. *J. Electrochem. Soc.* **148**, G297 (2001).
3. Yazdi, G. R., Iakimov, T. & Yakimova, R. Epitaxial graphene on sic: a review of growth and characterization. *Crystals* **6**, 53 (2016).
4. Rohlfing, M. & Pollmann, J. Dielectric function and reflectivity spectrum of SiC polytypes. *Phys. Rev. B* **63**, 125201 (2001).
5. Logothetidis, S. & Petalas, J. Dielectric function and reflectivity of 3C-silicon carbide and the component perpendicular to the *c* axis of 6H-silicon carbide in the energy region 1.5–9.5 eV. *J. Appl. Phys.* **80**, 1768–1772 (1996).
6. Weingärtner, R. et al. Determination of charge carrier concentration in n- and p-doped SiC based on optical absorption measurements. *Appl. Phys. Lett.* **80**, 70–72 (2002).
7. Zhang, X. & Kioupakis, E. Phonon-assisted optical absorption of SiC polytypes from first principles. *Phys. Rev. B* **107**, 115207 (2023).
8. Brudnyi, V. & Kosobutsky, A. V. Electronic structure and the local electroneutrality level of SiC polytypes from quasiparticle calculations within the *GW* approximation. *J. Exp. Theor. Phys.* **114**, 1037–1042 (2012).
9. Zhao, G. L. & Bagayoko, D. Electronic structure and charge transfer in 3C- and 4H-SiC. *N. J. Phys.* **2**, 16 (2000).
10. Cannuccia, E. & Gali, A. Thermal evolution of silicon carbide electronic bands. *Phys. Rev. Mater.* **4**, 014601 (2020).
11. Hsueh, H. C., Guo, G. Y. & Louie, S. G. Excitonic effects in the optical properties of a SiC sheet and nanotubes. *Phys. Rev. B* **84**, 085404 (2011).
12. Gao, W. et al. Quasiparticle energies and optical excitations of 3C-SiC divacancy from *GW* and *GW* plus Bethe–Salpeter equation calculations. *Phys. Rev. Mater.* **6**, 036201 (2022).
13. Hass, J. et al. Structural properties of the multilayer graphene/$4h-\mathrm{SiC}(000\bar{1})$ system as determined by surface X-ray diffraction. *Phys. Rev. B* **75**, 214109 (2007).
14. Emtsev, K. V. et al. Towards wafer-size graphene layers by atmospheric pressure graphitization of silicon carbide. *Nat. Mater.* **8**, 203–207 (2009).
15. Forbeaux, I., Themlin, J.-M. & Debever, J.-M. High-temperature graphitization of the 6H-SiC (0001) face. *Surf. Sci.* **442**, 9–18 (1999).
16. Zhao, J. et al. Ultra-high mobility semiconducting epitaxial graphene on silicon carbide. *Nature* **625**, 60–65 (2024).
17. Berger, C. et al. Electronic confinement and coherence in patterned epitaxial graphene. *Science* **312**, 1191–1196 (2006).
18. Chabi, S., Chang, H., Xia, Y. & Zhu, Y. From graphene to silicon carbide: ultrathin silicon carbide flakes. *Nanotechnology* **27**, 075602 (2016).
19. Polley, C. M. et al. Bottom-up growth of monolayer honeycomb SiC. *Phys. Rev. Lett.* **130**, 076203 (2023).
20. Giannazzo, F. Insight into the mechanisms of chemical doping of graphene on silicon carbide. *Nanotechnology* **27**, 072502 (2016).
21. Lin, Y.-M. et al. 100-GHz transistors from wafer-scale epitaxial graphene. *Science* **327**, 662–662 (2010).
22. Dawlaty, J. M. et al. Measurement of the optical absorption spectra of epitaxial graphene from terahertz to visible. *Appl. Phys. Lett.* **93**, 131905 (2008).
23. Peng, X. & Ahuja, R. Symmetry breaking induced bandgap in epitaxial graphene layers on sic. *Nano Lett.* **8**, 4464–4468 (2008).
24. Varchon, F. et al. Electronic structure of epitaxial graphene layers on SiC: effect of the substrate. *Phys. Rev. Lett.* **99**, 126805 (2007).
25. Mattausch, A. & Pankratov, O. Ab initio study of graphene on sic. *Phys. Rev. Lett.* **99**, 076802 (2007).
26. Hass, J. et al. Highly ordered graphene for two dimensional electronics. *Appl. Phys. Lett.* **89**, 143106 (2006).
27. Cimatti, I. et al. Vanadyl phthalocyanines on graphene/SiC(0001): toward a hybrid architecture for molecular spin qubits. *Nanoscale Horiz.* **4**, 1202–1210 (2019).
28. Yamasaki, S., Nakai, H., Murayama, K., Ohno, Y. & Nagase, M. Electron transfer characteristics of amino acid adsorption on epitaxial graphene FETs on SiC substrates. *AIP Adv.* **12**, 105310 (2022).
29. Kumar, A. et al. Charge-transfer-driven nonplanar adsorption of F4TCNQ molecules on epitaxial graphene. *ACS Nano* **11**, 4960–4968 (2017).
30. Stradi, D. et al. Understanding the self-assembly of TCNQ on Cu(111): a combined study based on scanning tunnelling microscopy experiments and density functional theory simulations. *RSC Adv.* **6**, 15071–15079 (2016).
31. Coletti, C. et al. Charge neutrality and band-gap tuning of epitaxial graphene on SiC by molecular doping. *Phys. Rev. B* **81**, 235401 (2010).
32. Chi, M. & Zhao, Y.-P. First principle study of the interaction and charge transfer between graphene and organic molecules. *Comput. Mater. Sci.* **56**, 79–84 (2012).
33. Otero, R., Miranda, R. & Gallego, J. M. A comparative computational study of the adsorption of TCNQ and F4-TCNQ on the coinage metal surfaces. *ACS Omega* **4**, 16906–16915 (2019).
34. de Oliveira, I. S. S. & Miwa, R. H. Organic molecules deposited on graphene: a computational investigation of self-assembly and electronic structure. *J. Chem. Phys.* **142**, 044301 (2015).
35. Neaton, J. B., Hybertsen, M. S. & Louie, S. G. Renormalization of molecular electronic levels at metal–molecule interfaces. *Phys. Rev. Lett.* **97**, 216405 (2006).
36. Hedin, L. New method for calculating the one-particle Green's function with application to the electron-gas problem. *Phys. Rev.* **139**, A796–A823 (1965).
37. Martin, R. M., Reining, L. & Ceperley, D. M.*Interacting Electrons: Theory and Computational Approaches* (Cambridge University Press, 2016).
38. Alaal, N., Loganathan, V., Medhekar, N. & Shukla, A. First principles many-body calculations of electronic structure and optical properties of SiC nanoribbons. *J. Phys. D Appl. Phys.* **49**, 105306 (2016).
39. Alaal, N., Loganathan, V., Medhekar, N. & Shukla, A. From half-metal to semiconductor: electron-correlation effects in zigzag SiC nanoribbons from first principles. *Phys. Rev. Appl.* **7**, 064009 (2017).
40. Singh, A., Mahamiya, V. & Shukla, A. Defect-driven tunable electronic and optical properties of two-dimensional silicon carbide. *Phys. Rev. B* **108**, 235311 (2023).
41. Ramsdell, L. S. & Kohn, J. A. Developments in silicon carbide research. *Acta Crystallogr.* **5**, 215–224 (1952).
42. Sorieul, S. et al. Study of damage in ion-irradiated $\alpha$-sic by optical spectroscopy. *J. Phys. Condens. Matter* **18**, 8493 (2006).
43. Norimatsu, W. & Kusunoki, M. Selective formation of abc-stacked graphene layers on SiC(0001). *Phys. Rev. B* **81**, 161410 (2010).
44. Mansouri, M. Effects of vacancy-defected, dopant and the adsorption of water upon $Mn_2O_3$ and $Mn_3O_4$ (001) surfaces: a first-principles study. *Acta Phys. Pol. A* **133**, 1178–1185 (2018).
45. Mansouri, M., Casanova, D., Koval, P. & Sánchez-Portal, D. *GW* approximation for open-shell molecules: a first-principles study. *N. J. Phys.* **23**, 093027 (2021).
46. Mansouri, M., Koval, P., Sharifzadeh, S. & Sánchez-Portal, D. Molecular doping in the organic semiconductor diindenoperylene:

Insights from many-body perturbation theory. *J. Phys. Chem. C* **127**, 16668–16678 (2023).

47. Jacquemin, D., Duchemin, I. & Blase, X. Benchmarking the Bethe–Salpeter formalism on a standard organic molecular set. *J. Chem. Theory Comput.* **11**, 3290–3304 (2015).
48. Khvostenko, O. G., Kinzyabulatov, R. R., Khatymova, L. Z. & Tseplin, E. E. The lowest triplet of tetracyanoquinodimethane via UV–vis absorption spectroscopy with Br-containing solvents. *J. Phys. Chem. A* **121**, 7349–7355 (2017).
49. Kresse, G. & Furthmüller, J. Efficient iterative schemes for ab initio total-energy calculations using a plane-wave basis set. *Phys. Rev. B* **54**, 11169–11186 (1996).
50. Heyd, J., Scuseria, G. E. & Ernzerhof, M. Hybrid functionals based on a screened Coulomb potential. *J. Chem. Phys.* **118**, 8207–8215 (2003).
51. Blöchl, P. E. Projector augmented-wave method. *Phys. Rev. B* **50**, 17953–17979 (1994).
52. Grimme, S. Semiempirical GGA-type density functional constructed with a long-range dispersion correction. *J. Comput. Chem.* **27**, 1787–1799 (2006).
53. Tang, W., Sanville, E. & Henkelman, G. A grid-based Bader analysis algorithm without lattice bias. *J. Phys. Condens. Matter* **21**, 084204 (2009).
54. Giannozzi, P. et al. QUANTUM ESPRESSO: a modular and open-source software project for quantum simulations of materials. *J. Phys. Condens. Matter* **21**, 395502 (2009).
55. Hamann, D. R. Optimized norm-conserving Vanderbilt pseudopotentials. *Phys. Rev. B* **88**, 085117 (2013).
56. Deslippe, J. et al. BerkeleyGW: a massively parallel computer package for the calculation of the quasiparticle and optical properties of materials and nanostructures. *Comput. Phys. Commun.* **183**, 1269–1289 (2012).
57. Liu, X. et al. Pyrene-stabilized acenes as intermolecular singlet fission candidates: Importance of exciton wave-function convergence. *J. Phys. Condens. Matter* **32**, 184001 (2020).
58. Bruneval, F. et al. MOLGW 1: Many-body perturbation theory software for atoms, molecules, and clusters. *Comput. Phys. Commun.* **208**, 149–161 (2016).

## Acknowledgements

We thank Nazario Martín and David Écija for illuminating discussions in the early stages of this work. All calculations were performed at the Mare Nostrum Supercomputer of the Red Española de Supercomputación (BSC-RES) and the Centro de Computación Científica de la Universidad Autónoma de Madrid (CCC-UAM). This work has been supported by the European Research Council (ERC) under the European Union's Horizon 2020 research and innovation program (grant agreement no. 951224, TOMATTO), the Ministerio de Ciencia e Innovación MICINN (Spain) through the projects PID2022-138288NB-C31 and PID2022-138288NB-C33, the "Severo Ochoa" Program for Centres of Excellence in R&D (CEX2020-001039-S), and the "María de Maeztu" Program for Units of Excellence in R&D (CEX2018-000805-M).

## Author contributions

M.M. conceived the study and conducted the calculations. M.M., C.D., and F.M. discussed the results, provided feedback, and contributed to the manuscript preparation. F.M. supervised the entire project.

## Competing interests

The authors declare no competing interests.

## Additional information

**Supplementary information** The online version contains supplementary material available at https://doi.org/10.1038/s43246-024-00549-6.

**Correspondence** and requests for materials should be addressed to Masoud Mansouri.

**Peer review information** *Communications Materials* thanks Alok Shukla and the other, anonymous, reviewer(s) for their contribution to the peer review of this work. Primary Handling Editor: Aldo Isidori.